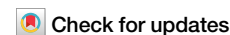




Predictability of tropical Pacific decadal variability is dominated by oceanic Rossby waves



Xian Wu¹✉, Stephen G. Yeager², Clara Deser², Antonietta Capotondi^{3,4}, Andrew T. Wittenberg⁵ & Michael J. McPhaden⁶

Despite its pronounced global impacts, tropical Pacific decadal variability (TPDV) is poorly predicted by current climate models due to model deficiencies and a limited understanding of its underlying mechanisms. Using observational data and a hierarchy of model simulations including decadal hindcasts, we find that decadal isopycnal depth variability driven by oceanic Rossby waves in the tropical Pacific provides the most important source of predictability for TPDV. The predictability arising from initial isopycnal depth conditions is further amplified by tropical ocean-atmosphere coupling and variations in the strength of subtropical cells in the Pacific throughout the decadal forecasts. Regional initialization experiments that effectively isolate the impact of different ocean basins on TPDV predictability highlight the essential role of the tropical Pacific. This study enhances our understanding of the mechanisms governing TPDV predictability, offering crucial insights for improving the accuracy of decadal predictions.

Decadal variations of sea surface temperature (SST) in the tropical Pacific can affect global hydroclimate and marine ecosystems^{1–3}, modulate global mean surface temperature changes^{4–6}, and interact with the El Niño–Southern Oscillation (ENSO) phenomenon, the leading mode of inter-annual climate variability^{7–11}. However, tropical Pacific decadal SST variations are poorly predicted by the Coupled Model Intercomparison Project Phase 5/6 (CMIP5/6) decadal retrospective forecasts, especially the internal tropical Pacific decadal variability (TPDV) associated with ocean initialization (after removing the effect from external forcings)^{12–14}. This low skill in the Pacific sector contrasts with the high skill for SST in most regions of the Indian and Atlantic Oceans, which has been attributed to the response to external forcing and/or ocean initialization^{12–15}.

The accuracy of decadal predictions of TPDV relies on the potential predictability provided by oceanic processes or external forcings, model representations of these mechanisms, and the realism of oceanic state estimates used to initialize the decadal forecasts. Achieving these conditions is challenging due to the complex processes that could affect TPDV^{11,16–19}, and systematic model biases in simulating the climatology, variability, and forced changes in the tropical Pacific, as well as their interactions with other ocean basins^{20–24}. Uncertainties in mechanistic understanding and model

biases of TPDV are challenging to reduce, given limited observational data, particularly for oceanic fields. Therefore, it remains difficult to determine to what extent the low decadal prediction skill for Pacific SSTs is due to intrinsic limits or deficiencies of forecast systems.

While numerous studies have investigated the complex origins and mechanisms of TPDV, less attention has been devoted to understanding whether and how these mechanisms provide sources of prediction skill in retrospective forecasts. The null hypothesis for TPDV is that it is a residual of ENSO decadal changes, which may themselves occur by chance. The leading Empirical Orthogonal Function (EOF) mode of TPDV shows a basin-wide ENSO-like spatial anomaly pattern (Fig. 1a) and is related to random changes in the relative number of warm (El Niño) and cold (La Niña) events over different epochs^{9,25}. The second EOF mode of TPDV displays a zonal dipole pattern in the tropical Pacific (Fig. S1a) and is associated with decadal modulation of ENSO amplitude or asymmetries^{7,26}. In contrast to these ENSO residual explanations, other studies suggest an extratropical contribution to TPDV from the North or South Pacific^{27–32}. In the extratropics, stochastic atmospheric variability can be integrated by the ocean due to its large thermal inertia, producing low-frequency SST variability^{33–36}. The resulting extratropical low-frequency SST variability,

¹Atmospheric and Oceanic Sciences Program, Princeton University, Princeton, NJ, USA. ²National Center for Atmospheric Research, Boulder, CO, USA.

³Cooperative Institute for Research in Environmental Sciences, University of Colorado Boulder, Boulder, CO, USA. ⁴National Oceanic and Atmospheric

Administration/Physical Sciences Laboratory, Boulder, CO, USA. ⁵National Oceanic and Atmospheric Administration/Geophysical Fluid Dynamics Laboratory, Princeton, NJ, USA. ⁶National Oceanic and Atmospheric Administration/Pacific Marine Environmental Laboratory, Seattle, WA, USA.

✉ e-mail: xw2794@princeton.edu

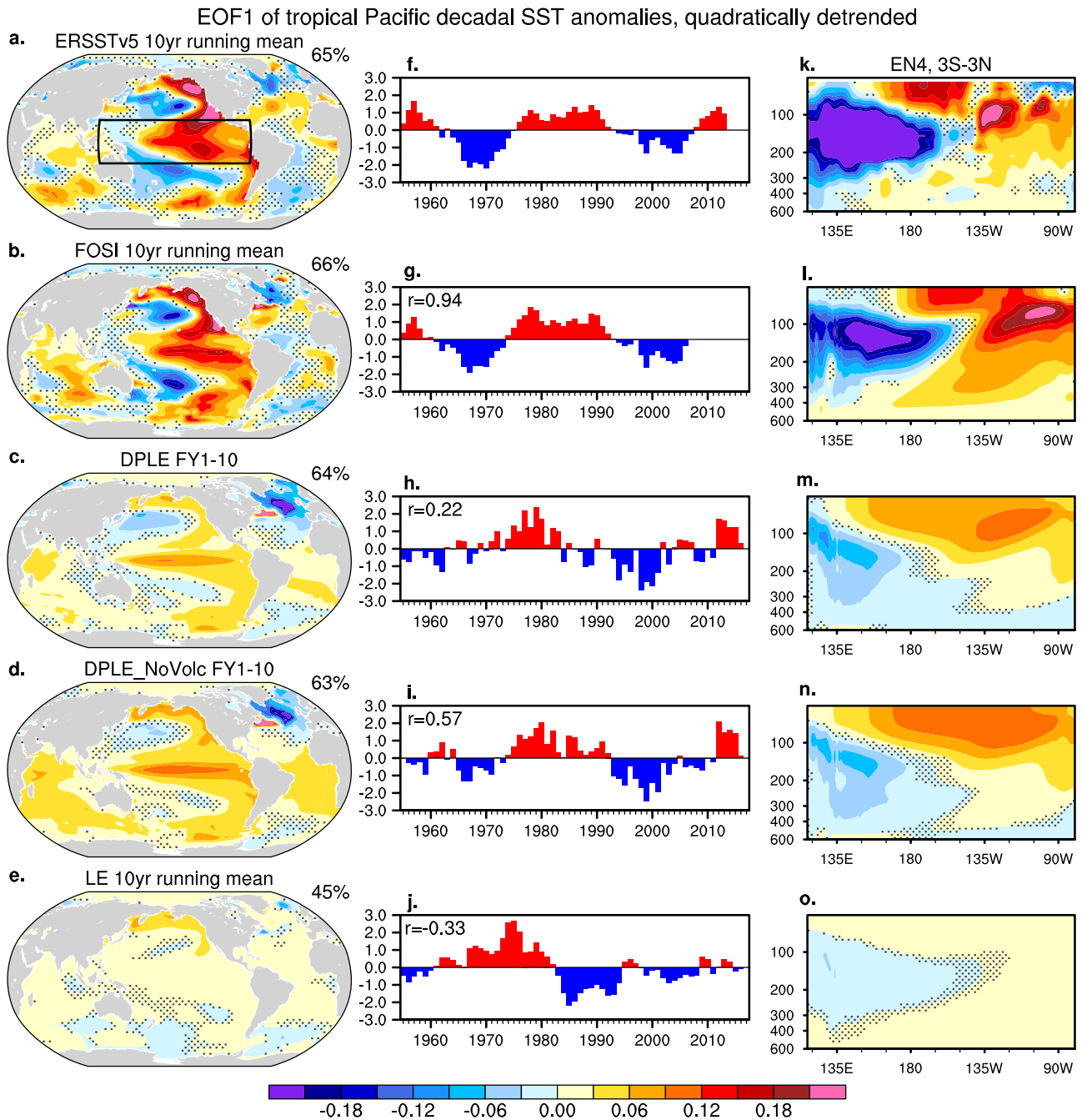


Fig. 1 | Tropical Pacific decadal variability from 1955 to 2022 in observations and CESM1 simulations/hindcasts. a–e Global SST and **(k–o)** equatorial Pacific subsurface ocean temperature patterns associated with TPDV in **(a, f, k)** observations (SST in ERSSTv5 and ocean temperature in EN4), **(b, g, l)** the forced ocean-sea ice simulation (FOSI), and the *ensemble-means* of **(c, h, m)** CESM1 DPLE, **(d, i, n)** DPLE_NoVolc, and **(e, j, o)** LE. The EOF analysis is conducted for *quadratically detrended and decadal* SST anomalies in the tropical Pacific (20°S–20°N, 120°E–80°W; outlined by the black box in **a**), with **(f–j)** showing the timeseries of the standardized first principal component (PC1). For the DPLE, DPLE_NoVolc, and LE datasets, the ensemble mean is computed first to estimate the predictable component of the system, followed by EOF analysis to extract the TPDV signal. The associated pattern is displayed using the regression of quadratically detrended and 10-year running-mean **(a–e)** SST anomalies and **(k–o)** equatorial Pacific (3°S–3°N) subsurface ocean temperature anomalies onto PC1. For **(a)** observations, **(b)** FOSI,

and **(e)** the ensemble mean of LE, the decadal SST anomalies are obtained by applying a 10-year running average filter to their continuous time series. For the ensemble-means of **(c)** DPLE and **(d)** DPLE_NoVolc, the decadal anomalies are derived by averaging forecasts during FY1–10 for each initialization date. The abscissa in **(f–j)** represents the start year of the 10-year averaging window (e.g., 1955 represents 10-year average anomalies spanning from 1955 to 1964 for observation, FOSI, and LE, and corresponds to the hindcasts averaged across FY1–10 initialized in Nov 1954 for DPLE and DPLE_NoVolc). The numbers in the top-right corner in **(a–e)** denote the percentage of total decadal variance explained by the leading EOF mode in each dataset. The stippling indicates regression values that are *not* significant at the 90% confidence level, based on a two-tailed Student’s *t*-test (see “Methods”). The *r* value indicates the correlations of each model simulation with observed PC1.

whose structures are referred to as South Pacific or North Pacific Meridional Modes (MMs) can then influence the tropical Pacific via thermodynamic and dynamical processes, particularly wind-evaporation-SST (WES) and low cloud-SST feedbacks, which contribute to the propagation of the MMs' wind stress and SST anomalies into the equatorial western-to-central Pacific^{30,31,37,38}.

Although the ENSO residual effect and stochastic atmospheric variability lack preferred timescales and are inherently unpredictable on decadal timescales³⁹, these random processes can initiate slow oceanic processes which likely determine the timescale of TPDV and provide a source of predictability^{11,18,19,40}. Based on observational and/or modeling studies, several oceanic mechanisms in the Pacific have been proposed to contribute to TPDV, including off-equatorial oceanic Rossby wave activity, spiciness advection, and variations in the strength of the subtropical cells (STCs). Decadal-scale off-equatorial oceanic Rossby wave reflections at the western boundary of the Pacific serve as a delayed negative feedback for TPDV by affecting equatorial Pacific thermocline depth, similar to the dynamics driving ENSO phase transitions on interannual timescales^{41–45}. STCs, upper-ocean overturning circulations connecting the subtropical and equatorial regions of the Pacific, influence tropical Pacific SSTs through mean advection of temperature anomalies ($\bar{v}T'$) or variations of STC strength ($\bar{v}\bar{T}$). Surface water masses in the subtropics that are subducted into the pycnocline may move equatorward and upwell to the surface upon reaching the equator, affecting the equatorial Pacific SSTs⁴⁶. However, subsequent studies suggest that this subtropical thermal subduction cannot efficiently reach the equator due to energy dissipation, dispersion in the form of planetary-scale oceanic waves, and perturbation from winds at lower latitudes⁴⁷. Density-compensated temperature anomalies, known as ocean "spiciness"⁴⁸, can propagate more effectively along isopycnal surfaces from the subtropics to the tropics^{49–52}. Alternatively, variations in STC strength can affect the *rate* of transport of the relatively constant water masses, influencing the equatorial Pacific upwelling, with enhanced upwelling bringing colder subsurface water to the surface and reduced upwelling having the opposite effect^{47,53–56}. The extent to which these various slow oceanic processes contribute to the predictability of TPDV and their relative importance remains unclear.

Other ocean basins may also influence tropical Pacific decadal climate through both atmospheric and oceanic pathways^{11,57}. For example, decadal-scale cooling in the central-eastern tropical Pacific, a main factor driving global surface warming slowdowns, has been linked to tropical Atlantic SST warming^{24,58–62}. However, some studies suggest that the tropical Atlantic's impact on the tropical Pacific might be overstated in regional SST-restoring experiments, which can overestimate the upward net surface heat fluxes in the tropical Atlantic compared to observations^{63,64}. Further, the Atlantic-Pacific connection may be artificially amplified by the way in which internal variability is defined, leading to spurious linkages⁶⁵. Investigations using an empirical model of the tropical Pacific-Atlantic systems, where the coupled inter-basin feedbacks can cleanly be isolated, indicate that Atlantic-Pacific coupling damps TPDV⁶⁶. Other studies also argue for the interaction between the tropical Indian and the tropical Pacific decadal climate^{67–70}. It is plausible that inter-basin interactions could play a role in TPDV predictions, but these linkages and causalities need to be verified with appropriate sensitivity experiments.

Despite the low real-world prediction skill, earlier studies based on perfect model experiments suggest potential multiyear predictability in the Pacific^{45,71}. Recent studies underscore the degradation of tropical Pacific decadal prediction skill by volcanic eruptions due to inadequate model representation of volcanic forcing and response, while forecast systems that exclude volcanic eruptions show high skill^{72–75}. Case studies indicate that particular phase transitions of TPDV can be retrospectively predicted when a model is properly initialized from strong ENSO event^{76,77}. Other studies indicate that spurious ENSO conditions due to initialization shock in the first forecast year will degrade the long-range skill of decadal hindcasts^{78,79}. Increasing the spatial resolution of decadal forecasts to resolve ocean eddies also improves the prediction skill in the *eastern* tropical Pacific because of a

more realistic prediction of the SST trend in the Southern Ocean and associated teleconnections⁸⁰. These findings collectively imply the presence of potential predictability for TPDV, which could arise from internal climate processes both within and beyond the Pacific.

Several important questions remain. What are the external (greenhouse gas, aerosols, and volcanic eruptions) and internal (oceanic initialization) factors affecting decadal prediction skill in the tropical Pacific? For the skill arising from internal oceanic initial conditions, what is the relative importance of the various mechanisms discussed above? Do other ocean basins play a role in affecting TPDV predictions? To answer these questions, we make use of observational and reanalysis data and a hierarchy of model simulations conducted with the Community Earth System Model version 1 (CESM1) at 1° horizontal resolution. In particular, we identify the precursory oceanic conditions for TPDV in observations and historical ocean-only simulations forced with observed surface conditions. We investigate both external and internal influences on TPDV prediction skill by comparing uninitialized historical simulations and initialized decadal retrospective forecasts. We focus on the initialized hindcasts conducted without volcanic forcing as these exhibit high prediction skill in the tropical Pacific⁷⁴, and attribute the predictability arising from initialization to specific oceanic processes. Finally, the impacts of different ocean basins on TPDV are discussed using a set of regional initialization experiments.

Results

Predictability and prediction skill of TPDV

We evaluate how observed TPDV during 1955–2022 is reproduced by a series of CESM1 simulations with varying levels of observational constraints (Fig. 1). We define TPDV as the leading EOF of quadratically-detrended 10-year running mean SST anomalies in the tropical Pacific (20°S–20°N; 120°E–80°W). This 10-year running mean is used to facilitate comparisons between observations and initialized forecasts as explained below, and it yields results similar to those using an 8–40-year band-pass filter¹¹. During 1955–2022, observed TPDV exhibits basin-wide SST anomalies in the tropical Pacific (Fig. 1a), fluctuating between warm and cold phases on decadal timescales (Fig. 1b). During the positive phase of TPDV, the thermocline becomes deeper in the eastern equatorial Pacific but shallower in the western part (Fig. 1c). The observed temporal and spatial features of TPDV are well reproduced by the ocean-sea ice simulation forced with observed surface forcing and fluxes (FOSI; Methods). Decadal Prediction Large Ensemble (DPLE) and DPLE without volcanic forcing (DPLE_NoVolc; Methods) are initialized from the FOSI oceanic and sea ice states on Nov 1 of each year during 1954–2015, and the ensemble-mean hindcasts are averaged over forecast year (FY) 1–10 for each initialization date, in order to examine the predictability of decadal anomalies. At FY1–10, DPLE_NoVolc shows a correlation skill [anomaly correlation coefficient (ACC) = 0.57] in predicting the observed (standardized) first principal component (PC1) timeseries of TPDV during 1955–2022, which is substantially higher than that for DPLE (ACC = 0.22). The 0.57 PC1 correlation between DPLE_NoVolc and observations indicates that over 30% of the observed PC1 variance is predictable with ocean initialization. The lower skill of DPLE compared to DPLE_NoVolc is related to an excessive tropical Pacific cooling response to large volcanic eruptions in the 1960s and 1980s, as suggested by Wu et al.⁷⁴. In contrast to the initialized decadal forecasts, the ensemble mean of the uninitialized CESM1 large ensemble (LE; Methods), which represents the model's response to external forcings, shows a negative correlation (−0.33) with the observed TPDV PC1 timeseries, and the magnitude of the externally forced TPDV PC1 is much weaker than TPDV PC1 in both the observations and initialized forecasts. This contrast between initialized CESM1 and uninitialized simulations suggests that the observed TPDV during the last ~70 years is largely driven by internal climate variability rather than external radiative forcing. We also present the same analysis for the second EOF mode in Fig. S1, which exhibits a zonal-dipole SST pattern over the tropical Pacific in observations and accounts for only 16% of the total decadal variance. The second PC (PC2) is linked to the

decadal modulation of ENSO characteristics and is poorly predicted by the decadal forecasts and the uninitialized simulations (Fig. S1h–j).

The ensemble-mean decadal hindcasts show weaker amplitude and excessive westward extension of TPDV SST anomalies compared to observations (Fig. 1a–d), due to the predictability limit of observed TPDV and/or inherent model bias. The magnitude of the global SST regression onto the standardized PC1 in the decadal hindcasts is weaker than observed for most of the ocean basins, mostly because the ensemble averaging reduces variance by isolating the predictable component of variance⁸¹. The free-running simulation of CESM1 under preindustrial conditions shows an amplitude of TPDV natural variability more comparable to that in observations (Fig. S2). The pattern bias of TPDV, however, exists even in the preindustrial control simulation (Fig. S2), suggesting that it arises from inherent biases in CESM1⁸². Despite the weaker predicted TPDV amplitude in DPLE and DPLE_NoVolc, the regressions of predicted SST anomalies onto PC1 over the subtropical North Atlantic and tropical Indian Oceans show amplitudes comparable to those in observations. It remains unclear whether this statistical relationship indicates stronger interbasin interactions in the decadal forecasts compared to observations, which will be investigated in a later section.

We also evaluate the SST and subsurface ocean temperature variability associated with TPDV in other observational or reanalysis datasets. ERSSTv5 and HadISST give similar results for SST, while EN4 and ORAS4 show differences in the amplitude and structure of equatorial Pacific subsurface temperature anomalies (cf. Fig. 1 and S2). In the following sections, we will present the results based on FOSI in the main text, and those based on observational datasets in the Supplementary Materials.

Consistent with the spatiotemporal features of TPDV captured by EOF analysis in the different simulations (Fig. 1), the ACC for detrended decadal SST anomalies in the tropical Pacific is increased by including ocean initialization (DPLE minus LE; Fig. 2e, j) or excluding volcanic forcing (DPLE_NoVolc minus DPLE; Fig. 2d, i). The ACC results are overall similar whether verifying against FOSI (Fig. 2) or observations (ERSSTv5 and EN4; Fig. S3). The increased skill in DPLE_NoVolc compared to DPLE is most pronounced over the central tropical Pacific, where the solar radiation reduction associated with volcanic aerosol forcing can most effectively influence the ocean mixed layer heat budget and SST⁷⁴. The skill enhancement by ocean initialization in DPLE relative to LE is confined to the eastern Pacific, due to intrinsic model bias in simulating excessive westward extension of TPDV SST anomalies. The local correlation skill for SST in the central-eastern Pacific reaches ~0.7 in DPLE_NoVolc, higher than that for EOF PC1 (0.57; Fig. 1).

We further investigate the ACC skill of ocean temperature in the equatorial Pacific as a function of depth and longitude (Fig. 2). The significant impact of volcanic forcing is limited to the upper ~100 m in the central equatorial Pacific (Fig. 2i), which is generally above the thermocline depth (black curve in Supplementary Fig. S4a). The influence of volcanic forcing on ocean temperatures is largely confined above the thermocline depth and acts primarily through shortwave radiation and ENSO dynamical processes⁷⁴. This suggests that the same subsurface oceanic process may operate in both DPLE and DPLE_NoVolc, but cannot provide a source of predictability for upper layer temperature and SST when the tropical Pacific system is perturbed by volcanic forcing. Related to the western Pacific pattern bias in subsurface temperatures (Fig. 1), ACC is insignificant (or even negative) in the western Pacific for the upper 250 m. In subsequent sections, we will explore the oceanic processes contributing to the predictable component of TPDV.

Pacific oceanic mechanisms contributing to TPDV predictability

In this section, we will determine if three leading oceanic mechanisms (Rossby waves, spiciness, and STCs) serve as precursors for TPDV in FOSI via statistical analysis and confirm their influence in the decadal hindcasts. We illustrate the characteristics of the Rossby wave reflection mechanism by showing variability of the depth of the $\sigma_{\theta} = 25.5 \text{ kg m}^{-3}$ isopycnal (Fig. S4; see “Methods” for the choice of this metric). To isolate the low-frequency

variability associated with TPDV (Fig. 3a), we use a 10-year running mean filter to smooth the annual mean fields that are dominated by ENSO variance (Fig. S5). However, in contrast to the equatorial Pacific where ENSO variability dominates, off-equatorial Pacific subsurface temperature shows more pronounced decadal variability (Fig. S4h). In addition, off-equatorial Pacific isopycnal depth shows robust decadal variations even in unfiltered data (Fig. S5).

During the positive phase of TPDV, decadal SST warming in the central-to-eastern equatorial Pacific (3°S–3°N; ~160°E–80°W) is concurrent with isopycnal deepening and vice versa during the negative phase of TPDV in FOSI (Fig. 3a). Phase changes of TPDV SST anomalies occurred around 1962, 1977, and 1997 (note that the year in the y-axis in Fig. 3a denotes the start year of the 10-year average). These SST phase changes were preceded by isopycnal depth anomalies propagating along the equator from the western to the eastern Pacific. These precursor isopycnal depth anomalies in the western equatorial Pacific are further linked to off-equatorial (10°–15°) isopycnal depth anomalies. The results suggest that there might be a delayed oceanic feedback contributing to TPDV phase changes. During the positive phase of TPDV, positive (10°–15°N) and negative (15°–10°S) wind stress curl anomalies generate off-equatorial upwelling Rossby waves. These waves propagate toward the western boundary of the Pacific, then travel equatorward along the western boundary (130°–135°E or 155°–160°E zonally averaged) and reflect as upwelling equatorial Kelvin waves (3°S–3°N), which may cause thermocline shoaling and SST cooling in the eastern equatorial Pacific.

In FOSI, equatorial Pacific decadal SST anomalies are significantly correlated with the state of western equatorial Pacific isopycnal depth anomalies occurring more than 7 years earlier and with even 13 years earlier precursory isopycnal conditions in the off-equatorial Pacific (Fig. 3b, c). Similar results are found for decadal SST anomalies in the tropical Pacific (20°S–20°N; not shown). Analysis of observational data (ERSSTv5/EN4/ERA5 in Fig. S6; HadISST/ORAS4/NOAA20CRv3 in Fig. S7) shows similar results regarding preceding isopycnal depth conditions in the western equatorial Pacific influencing TPDV equatorial Pacific SST anomalies. However, in both EN4 and ORAS4, isopycnal variability south of the equator makes a more important contribution to western equatorial Pacific isopycnal depth variability (Figs. S6 and S7), in contrast to FOSI which shows a stronger contribution from the north (Fig. 3). This discrepancy in the relative importance of oceanic conditions in the south vs. the north between FOSI and observations is likely related to uncertainties in the wind stress data used to force the ocean model component of CESM1^{15,83} (cf. Figure 3 and Figs. S6 and 7), and differences in the ocean solutions, assimilation, and statistical correction methods used in the observational datasets. Considerable differences also exist in subsurface temperature and salinity fields between EN4 and ORAS4, surface wind stress between ERA5 and 20CR, and SST fields between ERSSTv5 and HadISST (Figs. S6, 7). These observational uncertainties emphasize the need for improved ocean observations and data assimilation methods to better understand the mechanisms of TPDV.

Next, we compare TPDV SST anomalies with STC strength, estimated using the maximum of the Pacific zonally integrated interior (excluding the western boundary currents) meridional overturning circulation (MOC) streamfunction (see “Methods”) as a function of latitude in FOSI (Fig. 4a; positive/negative overturning streamfunction anomalies north/south of the Equator indicate poleward anomalous near-surface transport and intensification of STC). The vertical structure of STC climatology and anomalies during different TPDV phases are shown in Fig. S8. During the positive phase of TPDV, the STC slows down, with the near-surface flow exhibiting anomalous equatorward convergence, and vice versa during the negative phase of TPDV. The total near-surface meridional transport convergence or divergence (e.g., near-surface meridional transport values at 9°S minus 9°N; Fig. 4b blue curves) tends to significantly lag the equatorial Pacific decadal SST anomalies by 2–3 years (Fig. 4b, c black curves) and may act to strengthen TPDV SST anomalies via modulation of equatorial upwelling once a TPDV phase change is initiated. The northern branch of the STC

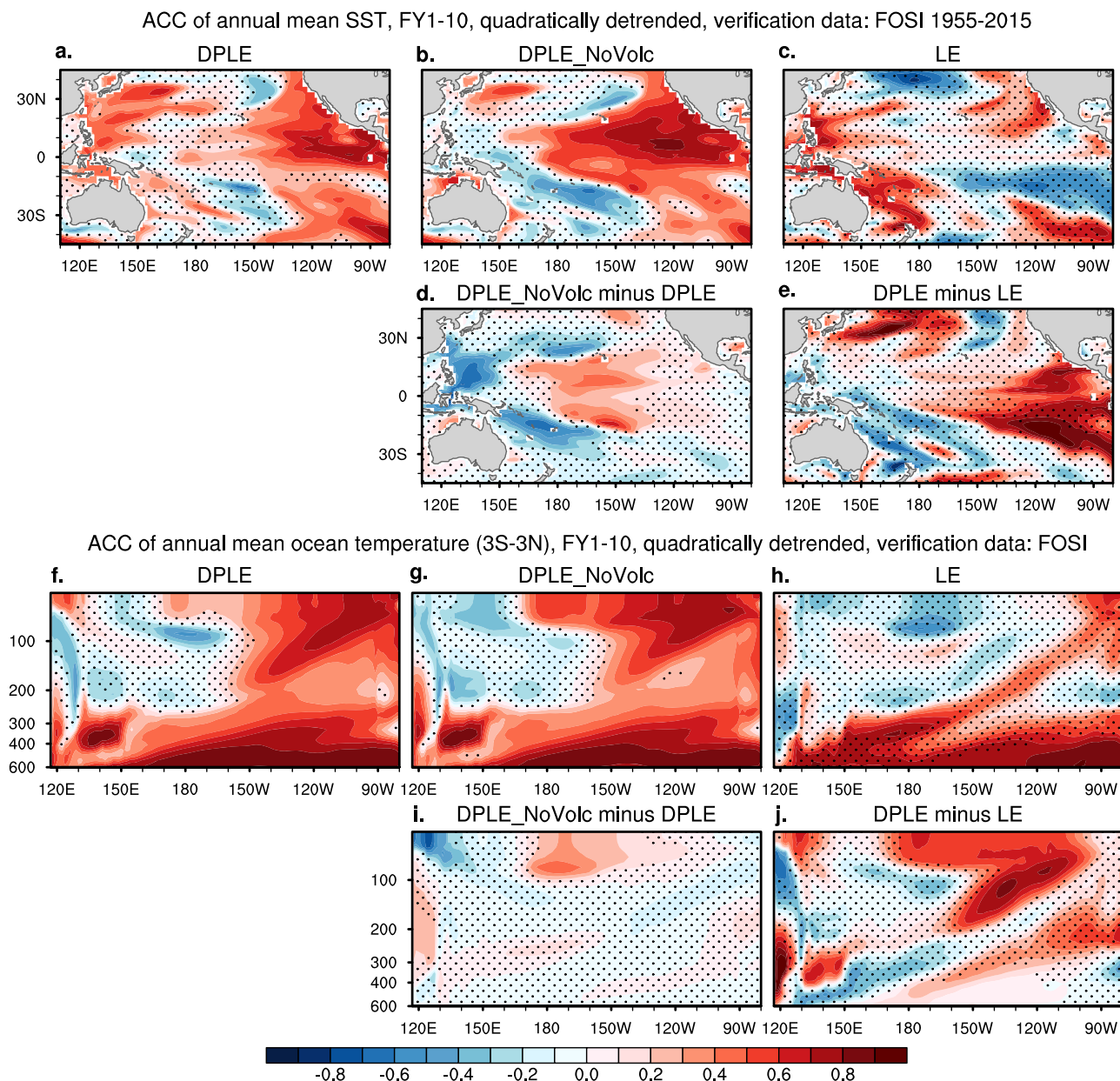


Fig. 2 | Decadal prediction skill is improved by ocean initialization and excluding volcanic forcing. Anomaly correlation coefficient (ACC) of quadratically detrended 10-year running-mean (a–e) SST and (f–j) equatorial Pacific (3°S–3°N) subsurface ocean temperature during 1955–2022 in the ensemble-mean forecasts averaged over FY1–10 for (a, f) DPLE and (b, g) DPLE_NoVolc, and 10-year running-mean

ensemble mean of (c, h) LE, and their differences [(d, i) DPLE_NoVolc minus DPLE, and (e, j) DPLE minus LE]. The ACC skill is verified against FOSI (see Fig. S3 for ACC skill verified against observations). Stippling indicates ACC or ACC difference values that are *not* significant at the 90% confidence level, based on bootstrapping across both time and ensemble members (see “Methods”).

(Fig. 4b, c yellow curves) makes a stronger contribution and exhibits a significantly stronger lag correlation with TPDV compared to the southern branch (green curves) in FOSI. Changes in the STC strength are not independent of the westward propagation of Rossby waves, which alter the zonal slope of the pycnocline and create meridional geostrophic current anomalies⁵⁶. Consequently, the collective effect of Rossby wave propagation causes a lag in zonally integrated interior meridional streamfunction variations relative to SST variations⁵⁶. Similar results are found using zonally integrated total transport across the Pacific (including the western boundary currents; Fig. S8a, b), which may better capture the equilibrium STC response to surface wind stress forcing. This similarity could be attributed to our application of a 10-year running mean filter to the STC anomalies, which may reduce the differences between the transient and equilibrium responses.

To illustrate the effect of spiciness advection on TPDV, we present a latitude-time diagram of decadal temperature anomalies on the time-varying isopycnal depth surface $\sigma_{\theta} = 25.5 \text{ kg m}^{-3}$ (Fig. 4d). Spiciness anomalies originate in the subtropical eastern Pacific and propagate to the western tropical Pacific (the pathway is denoted in Fig. S4l). The spiciness of the western equatorial Pacific (5°S–5°N) is largely controlled by the advection from the South Pacific (5°S–0°; Fig. 4e) and tends to be out-of-phase with the equatorial Pacific SST anomalies (Fig. 4f). These subsurface spiciness anomalies thus damp TPDV SST anomalies when they are brought to the surface by equatorial upwelling. Based on the diagnostic analyses shown in Figs. 3 and 4, isopycnal depth variability and associated Rossby wave activity appear to be the most important precursors for TPDV during 1948–2015 in FOSI.

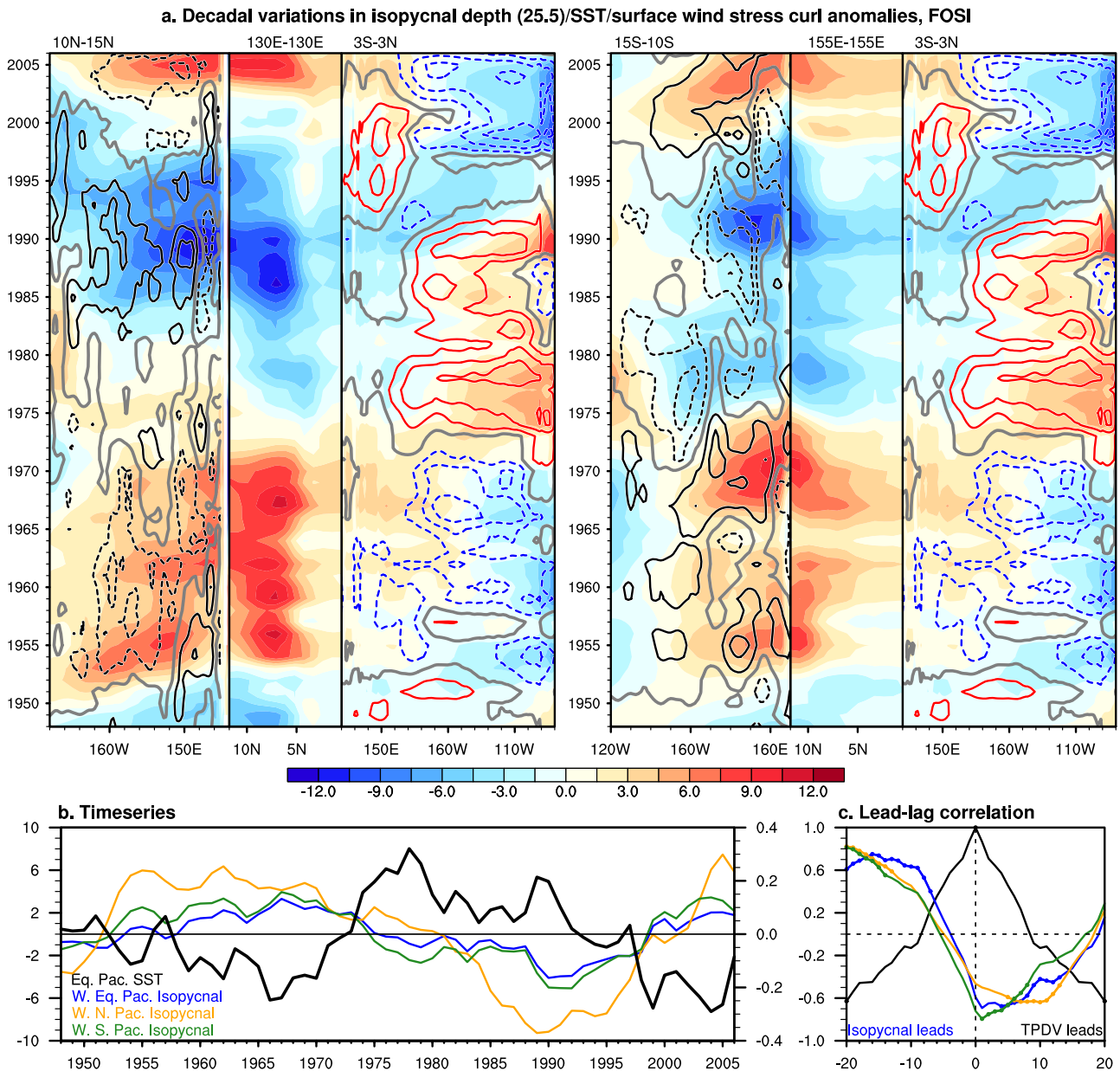


Fig. 3 | Relation of oceanic Rossby wave reflection to TPDV in FOSI. a Longitude-time sections of quadratically detrended and 10-year running-mean isopycnal depth anomalies (m; shading) along the off-equatorial (10°–15°N and 15°–10°S), western Pacific boundary (130°–135°E and 155°–160°E), and equatorial (3°S–3°N) waveguides during 1948–2015 (The year value in the y-axis represents the start year of any 10-year averaging window). In the equatorial segment, SST anomalies (°C, contours at intervals of 0.1; positive contours in red solid, negative contours in blue dashed, and zero contours in thick gray) are overlaid. In the off-equatorial segment, wind stress curl anomalies (N m^{-3} ; contours at intervals of 0.5×10^{-8} ; positive contours in black solid, negative contours in black dashed, zero contours in thick gray) are overlaid and smoothed with a nine-point local smoothing. Note that the longitude axis is reversed for the off-equatorial segment to show Rossby wave reflection at the western boundary. **b** Timeseries of quadratically detrended and 10-year running-mean filtered SST anomalies (°C) in the equatorial Pacific (3°S–3°N, 180°–80°W;

thickened black curve; right y-axis), isopycnal depth anomalies (m) in the western equatorial Pacific (3°S–3°N, 120°E–160°W; blue curve; left y-axis), in the northern off-equatorial western Pacific (10°–15°N, 120°E–160°W; orange curve) and southern off-equatorial western Pacific (15°–10°S, 155°E–160°W; green curve). **c** Lead-lag correlation of the 10-yr running-mean equatorial Pacific SST anomalies with the 10-year running-mean isopycnal depth anomalies in the western equatorial Pacific (blue curve), in the northern off-equatorial western Pacific (orange curve) and southern off-equatorial western Pacific (green curve) during a range of 20 lead to lag years. Negative lags correspond to isopycnal depth anomalies leading the TPDV event peak; positive lags correspond to isopycnal depth anomalies lagging the TPDV event peak. The filled circles indicate correlations that are statistically significant at the 90% confidence level, based on a bootstrapping method (Methods).

To confirm the role of different oceanic processes in the decadal hindcasts, we correlate the predicted equatorial Pacific SST in FY1–10 (representing TPDV) during 1955–2016 with concurrent oceanic fields in FY1–10 of DPLE_NoVolc (Fig. 5a–c) and the corresponding initial conditions in November (Nov0) in FOSI during 1954–2015 (Fig. 5d–f). In FY1–10, positive decadal SST anomalies in the tropical Pacific are associated

with isopycnal deepening in the eastern equatorial Pacific and shoaling in the west (Fig. 5a–c). The predicted equatorial Pacific SST index in FY1–10 does not show significant correlations with the initial SST anomalies over most regions in the tropical Pacific. In contrast, it shows significant correlations with subsurface temperature anomalies in the western equatorial Pacific and with isopycnal depth anomalies not only over the equatorial

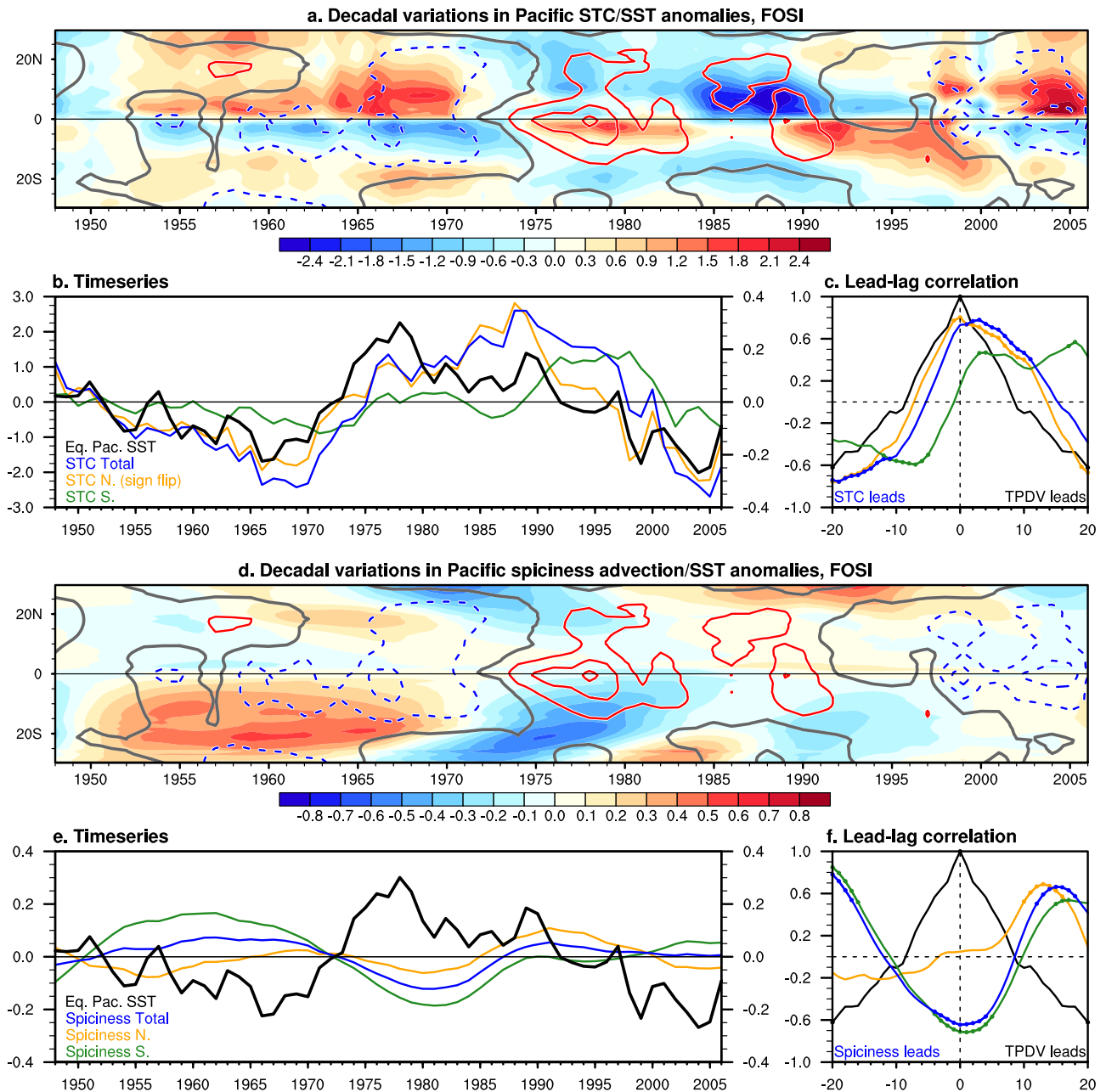


Fig. 4 | Relation of Pacific STC and spiciness anomalies to TPDV in FOSI.

a Latitude-time sections of quadratically detrended and 10-year running-mean filtered vertical maximum of the Pacific interior zonal average meridional overturning streamfunction (S_v ; shading; integrated from the Pacific eastern boundary to 145°E for the Northern Hemisphere and from the Pacific eastern boundary to 160°E for the Southern Hemisphere) and tropical Pacific (160°E–120°W) SST (°C; contours at intervals at 0.1; positive contours in red solid, negative contours in blue dashed, and zero contours in gray thickened) during 1948–2015 (The abscissa represents the start year of each 10-yr averaging window). **b** Timeseries of quadratically detrended and 10-year running-mean filtered SST (°C) anomalies in the equatorial Pacific (3°S–3°N, 180°–80°W; thickened black curve; right y-axis), STC (S_v) strength at 9°N (orange curve; sign flipped so that positive/negative values denote equatorward/poleward near-surface transport; left y-axis), 9°S (green curve), and the total

convergence/divergence between 9°N and 9°S (blue curve). **c** Lead-lag correlation of the equatorial Pacific SST anomalies in year 0 with the equatorial Pacific SST anomalies (black), STC strength at 9°N (orange curve), 9°S (green curve), and in total (blue curve) during a range of 20 lead to lag years. Positive (negative) lags indicate that TPDV leads (lags) the STC strength anomalies. The filled circles indicate correlations that are statistically significant at the 90% confidence level based on a bootstrapping method. **d** As in (a), but the shading indicates the spiciness anomalies (°C; left y-axis) along the path denoted by dots in Fig. S4l. **e** Timeseries of quadratically detrended and 10-year running-mean filtered SST (°C) anomalies in the equatorial Pacific as in (b), and spiciness anomalies (°C) along the advection pathway from panel d, meridionally averaged in the northern equatorial Pacific (0°–5°N; orange curve), southern equatorial Pacific (5°S–0°; green curve), and the total equatorial Pacific (5°S–5°N; blue curve). **f** As in (c), but spiciness anomalies in **e**.

western Pacific but also in the off-equatorial Pacific region (10°–20° latitude), suggesting the critical role of Rossby wave initialization.

To show the propagation and influence of subsurface processes through the 10-year forecast period in DPLE_NoVolc, we correlate the predicted equatorial Pacific SST index in FY5–10 with several fields at the

concurrent (FY5–10) and earlier 6-year forecast periods (FY4–9, 3–8, 2–7, and 1–6). This analysis reveals that equatorial Pacific SST anomalies in FY5–10 (Fig. 5g5) can be traced back to subsurface temperature anomalies in the equatorial Pacific (Fig. 5h1), along with off-equatorial and equatorial isopycnal depth anomalies in FY1–6 (Fig. 5i1). As significant SST

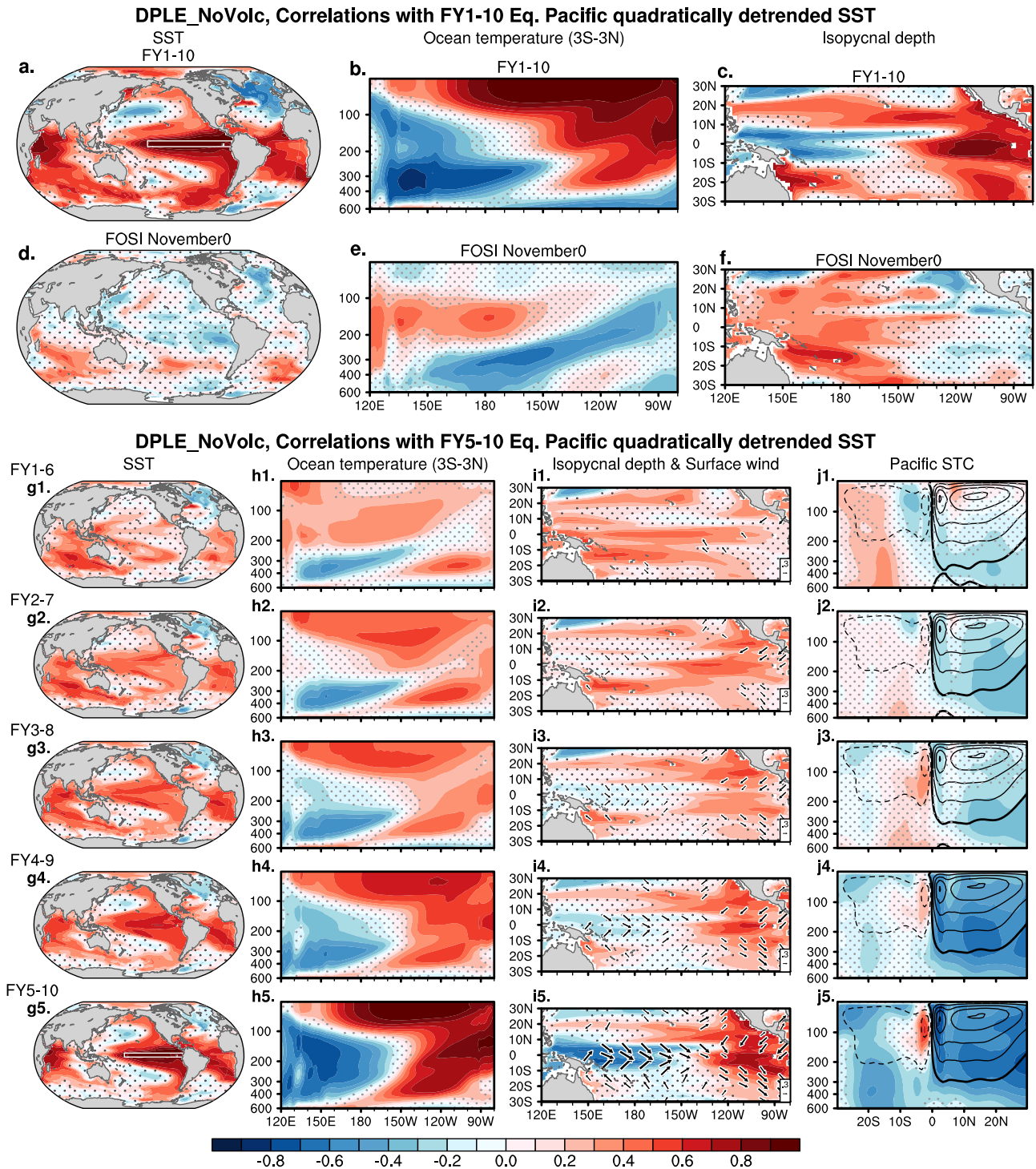


Fig. 5 | Source and persistence of predictability in initialized decadal forecasts. a–f Correlation maps with detrended SST anomalies in the central-eastern equatorial Pacific (3°S–3°N, 180°E–120°W; denoted by the white box in (a)) averaged in FY1–10 during 1955–2016 in DPLE_NoVolc. Correlations (color shading) are calculated with the quadratically detrended (a, d) global SST, (b, e) ocean temperature in the equatorial Pacific (3°S–3°N), and (c, f) tropical Pacific isopycnal depth ($\sigma_\theta = 25.5 \text{ kg m}^{-3}$) anomalies at (a–c) FY1–10 during 1955–2016, and (d–f) the corresponding FOSI initial conditions in Nov0 during 1954–2015. g–j Correlation maps with detrended SST anomalies in the central-eastern equatorial Pacific (3°S–3°N, 180°E–120°W; denoted by the white box in g5) averaged in FY5–10 during 1955–2016 in DPLE_NoVolc. Correlations (color shading) are

calculated with the detrended (g1–5) global SST, (h1–5) ocean temperature in the equatorial Pacific (3°S–3°N), (i1–5) tropical Pacific isopycnal depth ($\sigma_\theta = 25.5 \text{ kg m}^{-3}$), surface winds, and (j1–5) STC overturning streamfunction at FY1–6, FY2–7, FY3–8, FY4–9, and FY5–10 during 1955–2016. Drifting STC climatology in DPLE_NoVolc for the five FYs during 1964–2015 in are overlaid in j1–5 using black contours at intervals of 8 Sv [positive (negative) contours in solid (dashed) contours and zero contours thickened]. The stippling indicates shaded regression values that are *not* significant at the 90% confidence level, based on a two-tailed Student’s *t*-test (see “Methods”). Only significant correlations for surface wind vectors are shown.

correlations intensify in FY2–7 (Fig. 5g2), surface westerly anomalies start to develop over the western equatorial Pacific in FY3–8 (Fig. 5i2), deepening the isopycnal in the eastern equatorial Pacific (Fig. 5i2). The coupling of SST, wind, and isopycnal depth can enhance the predictability provided by the initial subsurface temperature anomalies. The equatorial Pacific SST index in FY5–10 also shows significant correlations with the Pacific STC overturning streamfunction, originating in the subsurface regions in the North (10°–20°N) and South (20°–10°S) Pacific in FY1–6 (Fig. 5j1). When a positive TPDV starts to develop at FY1–6, the negative overturning streamfunction anomalies in the subsurface North Pacific weaken the North Pacific branch of climatological clockwise STC (shown by positive values in solid contours). Similarly, the positive overturning streamfunction anomalies in the subsurface South Pacific weaken the South Pacific branch of climatological anticlockwise STC (shown by negative values in dashed contours). Both branches overamplify TPDV SST anomalies at later forecast times. In DPLe, however, tropical Pacific SST anomalies at FY5–10 show much weaker correlations with oceanic conditions at earlier lead times than in DPLe_NoVolc, suggesting that volcanic forcing perturbs the linkage between the initial condition memory and SST variability at later forecast times (Fig. S9).

Insignificant correlations between predicted TPDV SST anomalies at FY1–10 and initial tropical Pacific SST anomalies in Nov0 (Fig. 5) suggest that the initial ENSO state does not affect the overall TPDV predictability at 10-year lead. The minor role of ENSO is further examined using a Singular Value Decomposition (SVD) analysis⁸⁴ between predicted tropical Pacific SST and the global SST initial conditions in Nov0 (Fig. S10). The leading SVD mode (SVD1) explains 59% of the total squared covariance between predicted tropical Pacific SST and the global SST initial conditions. The timeseries of the two expansion coefficients of SVD1 show decadal variations, and the associated heterogeneous correlation maps onto the SVD timeseries closely mirror the linear correlation analysis in Fig. 5. In contrast, the two expansion coefficients of SVD2 show strong interannual variability associated with ENSO, accounting for 15% of the covariance. This result suggests that there is only a weak interannual component in the predicted tropical Pacific SST anomalies in FY1–10, manifesting as an equatorial SST mode affected by the initial ENSO states in Nov0. Although particular strong ENSO events have been suggested to trigger the phase transition of TPDV and provide a source of predictability^{76,77}, the causal contribution of ENSO to TPDV needs to be better verified and quantified.

Role of Interbasin interactions in affecting TPDV prediction during 1999–2008

In Fig. 5d, we also identify significant correlations between the predicted TPDV index and the initial SST conditions in several remote ocean areas, including negative correlations over the North Atlantic and positive correlations over the extratropical oceans of the Southern Hemisphere. To test if these correlations indicate causality, and to separate the effects of initial conditions in different ocean basins on the tropical Pacific predictions, we conduct a set of regional initialization experiments for the period 1999–2008 (Fig. 6b–e; “Methods”). During this period, the tropical Pacific shows negative decadal SST anomalies in observations (Fig. S11a) and FOSI (Fig. 6f), which are well predicted by the DPLe_NoVolc forecasts initialized on Nov 1, 1998, with different drift correction methods (Figs. S11b and 6g; See “Methods”). The comparisons among the sensitivity forecasts with regional ocean initialization suggest that this skillful prediction of tropical Pacific decadal cooling is mainly associated with tropical Pacific initialization (Fig. 6h), which shows negative isopycnal depth anomalies in the tropical Pacific in the initial conditions (Fig. S11c). The North Atlantic (20°N–60°N) initialization experiment produces positive SST anomalies over both the North Atlantic and northern tropical Atlantic (0°–20°N; Fig. 6d, i). In contrast to previous SST-restoring experiments e.g.,⁶², the tropical Atlantic-induced warming does not generate tropical Pacific cooling. This is because the net surface heat flux over the tropical Atlantic is downward (Fig. 6n), and so SST warming there is not an active forcing

that can affect atmospheric teleconnections, consistent with previous studies^{64,65}. The tropical Atlantic shows insignificant SST anomalies in the Full initialization experiment (Fig. 6g), possibly due to competing effects from the tropical Pacific (Fig. 6h) and North Atlantic (Fig. 6i). The Southern Hemisphere ocean initialization (Southern Ocean, Indian Ocean, and Atlantic Ocean sectors) is responsible for the predicted warming over the Southern Ocean in the Full Initialization experiment (cf. Figure 6g, j). However, the sign of the predicted ensemble-mean Southern Ocean warming is opposite to that observed and seen in FOSI (Fig. S11a and Fig. 6f) and might contribute to the tropical Pacific warming in the SH initialization experiment (Fig. 6j). This suggests that the predicted tropical Pacific cooling in the Full initialization experiment might be underestimated due to prediction errors in the Southern Ocean.

Given that interbasin interactions may vary from case to case, additional regional initialization experiments with more start dates are required to robustly isolate the influence of different ocean basins on TPDV prediction skill in general. A more refined analysis of the role of different ocean regions is also necessary. For example, further experiments are needed to distinguish the impacts of isopycnal initial conditions in the equatorial vs. off-equatorial Pacific on TPDV prediction skill. Although the correlation analysis does not suggest an influence from initial North Pacific SST anomalies on TPDV prediction skill (Fig. 5d), this might be due to inherent model underestimation of the coupling between the extratropics and tropics⁸⁵. Similarly, additional experiments are required to isolate the role of the Indian Ocean. The significant correlations between the predicted TPDV index and the initial Indian SST conditions are confined to the extratropical South Indian Ocean, rather than the tropical region, which has been suggested as an important factor for TPDV^{67,68}. Notably, most areas of the Indian Ocean exhibit significant prediction skill in detrended SST in both decadal forecasts and LE, suggesting that the Indian Ocean decadal prediction skill is largely attributable to external forcing (Figs. S13 and S14). In the selected case study of 1999–2008, the cooling in the Indian Ocean is not well predicted by any of the experiments (Fig. 6g–j), potentially diminishing its influence on the tropical Pacific.

Discussion

Our study investigates a set of oceanic mechanisms (Rossby waves, spiciness, STCs, and interbasin interactions) that may provide a source of predictability for TPDV based on observations and a hierarchy of model simulations and hindcasts. Diagnostic analyses of observational data and FOSI suggest that TPDV SST anomalies are preceded by isopycnal depth variability and associated Rossby wave activity in the off-equatorial Pacific. In contrast, the Pacific STC lags TPDV SST anomalies and may contribute to the persistence of TPDV. The spiciness advection from the eastern subtropical Pacific to the western equatorial Pacific tends to be out of phase with TPDV SST anomalies and potentially damps them. When initialized with the oceanic conditions provided by FOSI, the CESM1 decadal prediction system without volcanic forcing (DPLe_NoVolc) shows high skill in predicting observed TPDV during the 1950s to the present. Consistent with statistical relationships identified from diagnostic analyses, the high predictability of TPDV in DPLe_NoVolc arises from subsurface ocean initial conditions, particularly decadal isopycnal depth variability associated with oceanic Rossby wave adjustments in the tropical Pacific. The predictability inherent in the initial isopycnal conditions is further reinforced by the response of the subtropical cells and ocean-atmosphere coupling processes in the tropical Pacific throughout the 10-year forecasts.

Although we can rely on initial isopycnal anomalies for useful TPDV prediction skill, the origins of decadal isopycnal depth variability and the associated surface wind stress fluctuations driving isopycnal variability remain less clear, as also suggested by Capotondi et al.¹⁹. It remains unclear if this off-equatorial wind forcing arises from extratropical processes (such as atmospheric noise or coupled PMM) or teleconnections induced by tropical decadal SST anomalies¹⁹. In the CESM1 decadal forecasts, we find that the

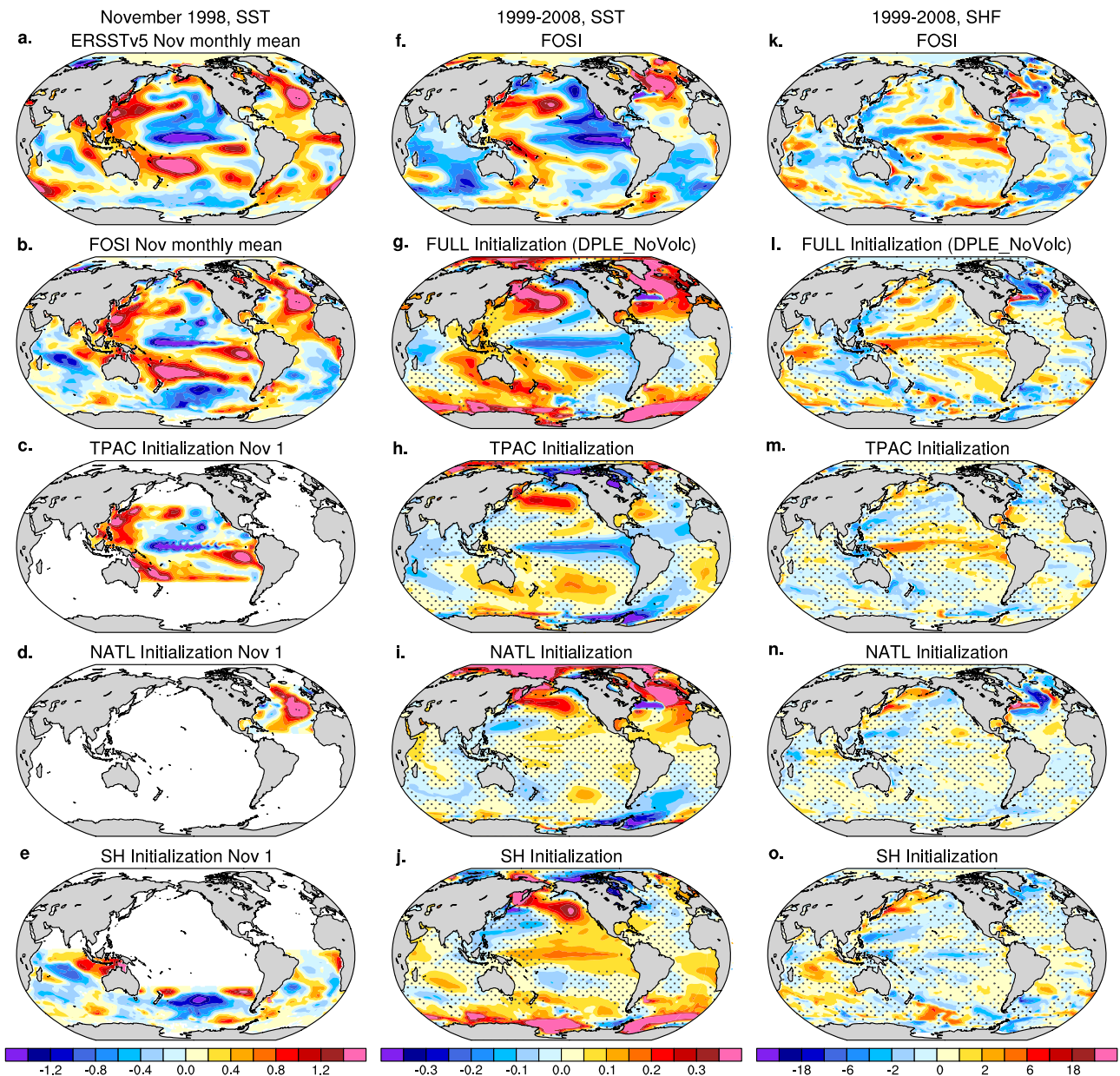


Fig. 6 | The influence of different ocean basins on TPDV predictability during 1999–2008. SST (°C) anomalies in November 1998 in (a) ERSSTv5 and (b) FOSI. c–e The areas with SST values on November 1 of 1998 denote the ocean regions that have the initialization of full-depth ocean temperature and salinity anomalies added on the climatology from FOSI; the November 1 FOSI climatology during 1954–2015 is used everywhere else. Quadratically detrended SST (°C) anomalies during

1999–2008 in (f) FOSI and 10-member ensemble mean forecasts initialized on November 1st, 1998, including (g) Full initialization experiment, (h) Tropical Pacific initialization, (i) North Atlantic initialization, and (j) Southern Ocean initialization. (k–o) as in (f–j) but for the surface net heat flux (SHF; $W\ m^{-2}$; positive values heat the ocean). Stippling indicates values that are *not* significant at the 90% confidence level, based on bootstrapping across ensemble members (see “Methods”).

initial ENSO SST state in a particular year plays a very minor role in affecting the overall TPDV predictability, but ENSO decadal modulation may contribute to establishing decadal wind and isopycnal variability in the off-equatorial Pacific.

To investigate the potential role of inter-basin interactions in TPDV prediction skill, we conducted regional initialization experiments which suggest that the predictability of TPDV SST cooling during 1999–2008 arises mainly from initial conditions in the tropical Pacific as opposed to those in the North Atlantic or tropical Atlantic. This result adds to previous work highlighting potential issues in using SST-restoring experiments to study the causality of interbasin ocean interactions⁶⁴. During 1999–2008, CESM1 decadal forecasts erroneously predict positive decadal SST anomalies in the Southern Ocean, which are opposite to those observed and

may contribute to an erroneous tropical Pacific SST warming. The Southern Ocean errors could be reduced by increasing the model resolution used for decadal hindcasts, which enhances prediction skill in the tropical Pacific⁸⁰. On the other hand, some studies suggest that models may underestimate Atlantic-Pacific Ocean interactions due to climatological biases, which displace atmospheric convective regimes and sensitivities^{23,86}. The influence of interbasin ocean interactions on decadal predictability needs to be further analyzed using regional experiments with more initialization dates and other properly designed experiments.

Our study provides an overview of both external and internal factors that may influence TPDV from a predictive perspective, but more detailed analyses and experiments are necessary to thoroughly investigate each of these factors. Our results are subject to observational uncertainties and to

biases in the single model we used, CESM1 at 1° resolution. Enhancing the spatial and temporal coverage of observational and reanalysis datasets is crucial for studying decadal climate variability. Future studies should explore the dependence of TPDV predictability on model physics and parameterizations, model resolution, and observational datasets. Although 1° horizontal resolution data products have been commonly used in decadal climate research due to their lower computational cost and longer data coverage, they may miss important features that can be resolved in higher-resolution datasets. For example, while decadal oceanic Rossby wave propagation associated with TPDV is likely to be robust in 1° resolution simulations, other processes, such as extratropical atmospheric variability, tropical-extratropical interactions, interbasin interactions, and ENSO modulations, may be sensitive to model resolution. Recent studies have demonstrated that high-resolution simulations improve the representation of coupled ocean-atmosphere processes in the North Pacific and tropical North Atlantic, potentially extending TPDV predictability limits^{87,88}. However, high-resolution CESM1 decadal forecasts do not improve central Pacific TPDV skill compared to DPLE at 1°, both of which suffer from errors from associated volcanic forcing^{74,80}. Further high-resolution experiments would be valuable to isolate these influences but remain very expensive to conduct. Moreover, it is important to test the dependence of our results using other CMIP6 decadal forecasts⁸⁹ as well as Ocean Model Inter-comparison Project simulations⁹⁰. Addressing the low CMIP5/6 decadal prediction skill in the Pacific Ocean is key for improving the skill of current decadal climate prediction systems, which bridge the gap between seasonal forecasts and centennial climate projections and provide useful information on climate adaptation and resilience for decision makers in many sectors of the economy.

Methods

a. CESM1 simulations and forecasts

We analyze the dynamics and predictability of TPDV using the CESM1, a global Earth system model consisting of atmosphere, ocean, land, and ice components linked by a flux coupler⁹¹. All experiments are conducted using the same model version as in the 40-member CESM1 Large Ensemble (CESM1 LE⁹²) at nominal 1° latitude-longitude resolution, including the Community Atmosphere Model, version 5 (CAM5⁹³) with 30 vertical levels; the Parallel Ocean Program, version 2⁹⁴ with 60 vertical levels; the Community Land Model, version 4⁹⁵; and the Los Alamos National Laboratory Community Ice Code, version 4⁹⁶. TPDV characteristics have been investigated in preindustrial and historical simulations conducted with several versions of CESM, which realistically simulate key statistics⁹⁷ and oceanic processes³⁰ (e.g., Rossby wave reflection) but exhibit deficiencies in representing tropical-extratropical interactions⁸⁵.

To compensate for the lack of comprehensive and consistent observations and reanalysis of subsurface oceanic processes that could influence TPDV, we analyze a forced ocean-sea ice simulation (FOSI), in which the ocean and sea ice components are forced with observed atmospheric and surface flux fields. The surface fluxes are derived using bulk formulae based on observed atmospheric fields from the Coordinated Ocean-Ice Reference Experiment forcing dataset (Please refer to Yeager (2018)⁹⁸ for more details). FOSI provides a realistic simulation of SST variability during 1948–2015, despite some inconsistencies in the Southern Ocean⁹⁹ (Fig. S12). Estimates for subsurface ocean temperatures and salinities are subject to larger observational uncertainties than for SST, as discussed in the following result sections.

FOSI provides the ocean and sea ice conditions needed to initialize the DPLE¹⁵ and a parallel decadal forecast set that excludes historical volcanic aerosol forcing (DPLE_NoVolc⁷⁴). In DPLE, 40-member forecasts are initialized from identical oceanic and sea ice conditions from FOSI on November 1st of each year during 1954–2015 and integrated for 122 months. The atmosphere and land initial conditions are expected to play a very minor role in contributing to decadal-scale climate predictability, and are obtained from a random member of the CESM1 LE without any observational constraints except for the historical radiative forcing.

The ensemble spread among individual members is created by adding round-off level perturbations to the initial atmospheric temperatures. The CMIP5 historical forcings for 1954–2005, and representative concentration pathway (RCP) 8.5 forcings for 2006 and onwards, are used as the external forcings for the DPLE forecasts. DPLE_NoVolc follows the DPLE protocol, except that it excludes historical volcanic aerosol forcing during 1954–2005 and has a smaller ensemble size of 10. The comparison between DPLE and DPLE_NoVolc isolates the effect of historical volcanic forcing on decadal prediction skill and predictability⁷⁴.

To isolate the role of initialization in affecting predictability and prediction skill, we compare the DPLE with the uninitialized CESM1 LE¹⁵. The CESM1 LE is comprised of 40-member historical simulations subject to the CMIP5 forcings during 1920–2100, including the historical volcanic forcing⁹². We quadratically detrend all data sets (observed and simulated) to remove the forced climate change signal during 1954–2015. Results are very similar if we use other methods of estimating and removing the forced climate signal, including subtracting a linear trend or the ensemble mean of the CESM1 LE⁷⁴. We also evaluate the performance of CESM1 in simulating intrinsic TPDV variability in an 1801-yr CESM1 control simulation under preindustrial atmospheric greenhouse gas concentrations.

b. Observational datasets

We assess the simulation realism and retrospective forecast skill of TPDV using multiple observational and reanalysis datasets available from the 1950s to 2022. The SSTs are taken from the National Oceanic and Atmospheric Administration (NOAA) Extended Reconstruction Sea Surface Temperature version 5¹⁰⁰ (ERSSTv5) dataset at 2° spatial resolution, and the Hadley Centre Sea Ice and SST dataset¹⁰¹ (HadISST) at 1° spatial resolution, during 1954–2022. The ocean temperature and salinity are taken from the Met Office Hadley Center EN4¹⁰² (EN4) with bias correction¹⁰³ at 1° horizontal resolution with 42 vertical levels during 1954–2022, and the European Centre for Medium-Range Weather Forecasts (ECMWF) Ocean Reanalysis System 4¹⁰⁴ (ORAS4) at 1° horizontal resolution with 42 vertical levels during 1958–2017. The ocean potential density is calculated using the temperature and salinity based on the equation of state for seawater¹⁰⁵. Surface wind stress is taken from the fifth generation ECMWF atmospheric reanalysis of global climate¹⁰⁶ (ERA5) for 1954–2022. Surface wind stress is also calculated based on surface wind components from the NOAA Twentieth Century Reanalysis version 3¹⁰⁷ (NOAA20CrV3) during 1954–2015 for comparisons. All observational data are re-gridded to the model grid at ~1° using a bilinear interpolation before comparison.

c. Analysis methods

Decadal forecasts are initialized from full-field oceanic states constrained by observations and will drift toward the model's biased climatology as the forecasts progress. To obtain forecast anomalies, forecast lead-dependent climatologies are removed from each ensemble member. For each forecast year (FY) 1–10, a climatology is determined by averaging the ensemble mean annual mean forecasts at that lead across 1964–2015. The choice of the 1964–2015 period as the baseline climatology ensures a consistent sample size (52 years) for each lead time. This drift-correction method has been widely adopted in seasonal-to-decadal prediction studies, but the impact of systematic model error and initialization shock on prediction skill remains to be explored⁹⁹. Anthropogenic climate change is estimated as a quadratic fit of the ensemble mean forecast anomalies across 1954–2015, as a function of lead time (i.e., FY1–10). This estimated climate change signal is then subtracted from individual drift-corrected ensemble members, to obtain detrended forecast anomalies.

We evaluate the model performance in capturing observed TPDV using EOF analysis, and by calculating the anomaly correlation coefficient (ACC) between the ensemble-mean forecasts and observations. Statistical significance of the results is tested using a bootstrapping method^{15,108}. At each spatial location, we determine a nonparametric bootstrap distribution of the forecast ACC, ACC difference, correlation, or composite anomalies by resampling (with replacement) the forecast ensembles across both the time

and/or ensemble member dimensions, and then recalculating the statistics for each of the 5000 samples. The calculation of 5000 values is performed using 10-member ensembles for all model analyses, considering the varied ensemble sizes of DPLE (40 ensemble members), DPLE_NoVolc (10), and LE (40). A positive ACC or ACC difference value of ensemble-mean forecasts is deemed significant at the 90% confidence level if its bootstrapped distribution contains fewer than 500 values below zero ($p < 500/5000 = 0.1$), and vice versa for a negative value. The statistical significance of SST and subsurface ocean temperature regression coefficients on the PC timeseries (Figs. 1, S1 and S2) and the lead-lag regressions of various fields on the equatorial Pacific SST index (Fig. 5 and S9) are tested using a two-tailed Student's *t*-test. The equivalent degrees of freedom are calculated using the formula $N * (1 - r)/(1 + r)$, where *r* is the lag-one autocorrelation of the EOF PC time series or the equatorial Pacific SST time series.

Several metrics are used to examine oceanic processes relevant to TPDV. Mixed layer depth in CESM1-FOSI is a monthly model output defined using a maximum buoyancy gradient criterion¹⁰⁹. Monthly thermocline depth is calculated as the depth of the maximum vertical temperature gradient. We use the monthly isopycnal depth where the potential density is equal to 25.5 kg m^{-3} ($\sigma_{\theta} = 25.5 \text{ kg m}^{-3}$) to capture the evolution of both off-equatorial and equatorial oceanic wave characteristics. The climatological depth of this isopycnal aligns closely with the depth where large variability of subsurface ocean temperature occurs for both equatorial (3°S – 3°N ; Fig. S4b) and off-equatorial (15°S – 20°N ; Fig. S4f) Pacific regions. Its vertical displacement mostly reflects adiabatic temperature variability associated with oceanic wave propagation, which is most pronounced at 10° – 15° latitude as shown in Fig. S3j and consistent with earlier studies^{110,111}. Additionally, this isopycnal ($\sigma_{\theta} = 25.5 \text{ kg m}^{-3}$) lies below the equatorial Pacific thermocline and can remain unaffected by volcanic forcing during a 10-year forecast period (Fig. 2; Fig. S4a). STC transports are defined as interior MOC streamfunction integrated from the Pacific eastern boundary to 145°E for the Northern Hemisphere and from the eastern boundary to 160°E for the Southern Hemisphere⁵³. The MOC streamfunction is calculated offline using the CESM model output of meridional and vertical velocities (Eulerian-mean, submesoscale, and Bolus velocity components) for FOSI, DPLE, and DPLE_NoVolc. Spiciness is defined using the monthly temperature along the time-dependent monthly isopycnal surface where $\sigma_{\theta} = 25.5 \text{ kg m}^{-3}$.

d. Regional initialization experiments

To examine the impact of initial ocean conditions in different ocean basins on TPDV predictions, we conducted a set of sensitivity experiments with regional initialization. We focus on the period of 1999–2008, during which the tropical Pacific exhibited negative decadal SST anomalies in observations. This tropical Pacific decadal cooling is well predicted by the DPLE_NoVolc forecasts initialized from the global oceanic states estimated by FOSI on November 1, 1998, with a ~ 10 -year lead. We refer to this DPLE_NoVolc forecast as the Global Initialization experiment (Fig. 6). To separate which part of the ocean initialization is more important to this prediction case, we conducted the following sensitivity experiments (Fig. 6): (1) A control ensemble initialized with the global FOSI climatology during 1954–2015 (Climatology initialization); (2) An ensemble initialized with the global FOSI climatology and full-depth ocean temperature and salinity anomalies in the North Atlantic (North Atlantic initialization; 20° – 60°N); (3) Similar to 2), but focusing on Tropical Pacific initialization (20°S – 20°N); and (4) Southern Hemisphere Ocean initialization, including the Southern Ocean, tropical Indian Ocean and tropical South Atlantic Ocean. To avoid discontinuities in oceanic forcing at the boundaries, we apply a linear interpolation over 5° latitude bands. Each experiment includes 10-member forecasts subject to external radiative forcings from November 1998 to December 2008, as was done for the Global Initialization experiment. Forecast anomalies are computed by subtracting the control simulation (Experiment 1) from Experiments 2–4 and the Global Initialization experiment. This approach to calculating forecast anomalies assumes a consistent time-dependent model drift across all experiments and is used to

prevent the extensive computing resources required to reproduce initialized forecasts for every year from 1954 to 2015 for each experiment. The forecast anomalies for the Global Initialization experiment, obtained by removing the control simulation, are very similar to the anomalies calculated using the traditional drift correction (Fig. S11b) and quadratic detrending (Fig. 6g).

Data availability

NCAR's Climate Data Gateway provides the output from CESM1 DPLE (<https://www.earthsystemgrid.org/dataset/ucar.cgd.cesm4.CESM1-CAM5-DP.html>), FOSI (https://www.earthsystemgrid.org/dataset/ucar.cgd.cesm4.DPLE-FOSI.ocn.proc.monthly_ave.html), and LE (<https://www.earthsystemgrid.org/dataset/ucar.cgd.cesm4.cesmLE.html>). DPLE_NoVolc is available through <https://portal.nersc.gov/archive/home/c/ccsm/www/CESM1-CAM5-DP-NoV>. Observational and reanalysis datasets used in this study are available online: ERSSTv5 SSTs from <https://psl.noaa.gov/data/gridded/data.noaa.ersst.v5.html>, HadISST from <http://www.metoffice.gov.uk/hadobs/>, ORAS4 from <ftp://ftp-icdc.cen.unihamburg.de/EASYInit/ORA-S4>, EN4 from <https://www.metoffice.gov.uk/hadobs/en4/download.html>, ERA5 from <https://www.ecmwf.int/en/forecasts/dataset/ecmwf-reanalysis-v5>, and NOAA20CRv3 from https://www.psl.noaa.gov/data/gridded/data.20thC_ReanV3.html.

Code availability

Codes generated during this study are available from the corresponding author upon reasonable request.

Received: 2 July 2024; Accepted: 19 November 2024;

Published online: 30 November 2024

References

- Di Lorenzo, E. et al. Synthesis of Pacific Ocean climate and ecosystem dynamics. *Oceanography* **26**, 68–81 (2013).
- Di Lorenzo, E. et al. Modes and mechanisms of Pacific decadal-scale variability. *Annu. Rev. Mar. Sci.* **15**, 249–275 (2022).
- Capotondi, A., Newman, M., Xu, T. & Di Lorenzo, E. An optimal precursor of northeast Pacific marine heatwaves and central Pacific El Niño events. *Geophys. Res. Lett.* **49**, e2021GL097350 (2022).
- Kosaka, Y. & Xie, S.-P. Recent global-warming hiatus tied to equatorial Pacific surface cooling. *Nature* **501**, 403–407 (2013).
- Meehl, G. A., Hu, A., Arblaster, J. M., Fasullo, J. & Trenberth, K. E. Externally forced and internally generated decadal climate variability associated with the interdecadal Pacific oscillation. *J. Clim.* **26**, 130408111212000 (2013).
- England, M. H. et al. Recent intensification of wind-driven circulation in the Pacific and the ongoing warming hiatus. *Nat. Clim. Chang.* **4**, 222–227 (2014).
- Rodgers, K. B., Friederichs, P. & Latif, M. Tropical Pacific decadal variability and its relation to decadal modulations of ENSO. *J. Clim.* **17**, 3761–3774 (2004).
- Vimont, D. J. The contribution of the interannual ENSO cycle to the spatial pattern of decadal ENSO-like variability. *J. Clim.* **18**, 2080–2092 (2005).
- Okumura, Y. M., Sun, T. & Wu, X. Asymmetric modulation of El Niño and La Niña and the linkage to tropical Pacific decadal variability. *J. Clim.* **30**, 4705–4733 (2017).
- Sun, T. & Okumura, Y. M. Impact of ENSO-like tropical Pacific decadal variability on the relative frequency of El Niño and La Niña events. *Geophys. Res. Lett.* **47**, e2019GL085832 (2020).
- Power, S. et al. Decadal climate variability in the tropical Pacific: characteristics, causes, predictability, and prospects. *Science* **374**, eaay9165 (2021).
- Doblas-Reyes, F. et al. Initialized near-term regional climate change prediction. *Nat. Commun.* **4**, 1715 (2013).
- Kirtman, B. et al. Near-term Climate Change: Projections and Predictability, Climate Change 2013: The Physical Science Basis.

- Contribution of Working Group I to the Fifth Assessment Report of the Intergovernmental Panel on Climate Change (eds Stocker, T. F., et al.) (2013).
14. Smith, D. et al. Robust skill of decadal climate predictions. *Npj Clim. Atmos. Sci.* **2**, 13 (2019).
 15. Yeager, S. et al. Predicting near-term changes in the Earth System: a large ensemble of initialized decadal prediction simulations using the Community Earth System Model. *Bull. Am. Meteorol. Soc.* **99**, 1867–1886 (2018).
 16. Meehl, G. A. et al. Decadal climate prediction: an update from the trenches. *B Am. Meteorol. Soc.* **95**, 243–267 (2014).
 17. Newman, M. et al. The Pacific decadal oscillation, revisited. *J. Clim.* **29**, 4399–4427 (2016).
 18. Liu, Z. & Di Lorenzo, E. Mechanisms and predictability of Pacific decadal variability. *Curr. Clim. Chang. Rep.* **4**, 128–144 (2018).
 19. Capotondi, A. et al. Mechanisms of tropical Pacific decadal variability. *Nat. Rev. Earth Environ.* 1–16. <https://doi.org/10.1038/s43017-023-00486-x> (2023).
 20. Guilyardi, E., Capotondi, A., Lengaigne, M., Thual, S. & Wittenberg, A. T. El Niño Southern oscillation in a changing climate. *Geophys. Monogr. Ser.* 199–226. <https://doi.org/10.1002/9781119548164.ch9> (2020).
 21. Lee, S. et al. On the future zonal contrasts of equatorial Pacific climate: perspectives from observations, simulations, and theories. *npj Clim. Atmos. Sci.* **5**, 82 (2022).
 22. Wills, R. C. J., Dong, Y., Proistosescu, C., Armour, K. C. & Battisti, D. S. Systematic climate model biases in the large-scale patterns of recent sea-surface temperature and sea-level pressure change. *Geophys. Res. Lett.* **49**, e2022GL100011 (2022).
 23. Li, C., Dommenges, D. & McGregor, S. Trans-basin Atlantic-Pacific connections further weakened by common model Pacific mean SST biases. *Nat. Commun.* **11**, 5677 (2020).
 24. McGregor, S. et al. Recent Walker circulation strengthening and Pacific cooling amplified by Atlantic warming. *Nat. Clim. Chang.* **4**, 888–892 (2014).
 25. Lin, R., Zheng, F. & Dong, X. ENSO frequency asymmetry and the Pacific decadal oscillation in observations and 19 CMIP5 models. *Adv. Atmos. Sci.* **35**, 495–506 (2018).
 26. Ogata, T., Xie, S.-P., Wittenberg, A. & Sun, D.-Z. Interdecadal amplitude modulation of El Niño–Southern Oscillation and its impact on tropical Pacific decadal variability. *J. Clim.* **26**, 130412124111006 (2013).
 27. Yeh, S.-W. & Kirtman, B. P. ENSO amplitude changes due to climate change projections in different coupled models. *J. Clim.* **20**, 203–217 (2007).
 28. Chung, C. T. Y., Power, S. B., Sullivan, A. & Delage, F. The role of the South Pacific in modulating tropical Pacific variability. *Sci. Rep.* **9**, 18311 (2019).
 29. Liguori, G. & Di Lorenzo, E. Separating the North and South Pacific meridional modes contributions to ENSO and tropical decadal variability. *Geophys. Res. Lett.* **46**, 906–915 (2019).
 30. Sun, T. & Okumura, Y. M. Role of stochastic atmospheric forcing from the South and North Pacific in tropical Pacific decadal variability. *J. Clim.* **32**, 4013–4038 (2019).
 31. Zhao, Y. & Di Lorenzo, E. The impacts of extra-tropical ENSO precursors on tropical Pacific decadal-scale variability. *Sci. Rep.* **10**, 3031 (2020).
 32. San, S.-C., Tseng, Y.-H., Ding, R. & Di Lorenzo, E. A key role of off-equatorial subsurface temperature anomalies in Tropical Pacific decadal variability. *npj Clim. Atmos. Sci.* **7**, 109 (2024).
 33. Hasselmann, K. Stochastic climate models Part I. Theory. *Tellus* **28**, 473–485 (1976).
 34. Frankignoul, C., Müller, P. & Zorita, E. A simple model of the decadal response of the ocean to stochastic wind forcing*. *J. Phys. Oceanogr.* **27**, 1533–1546 (1997).
 35. Schneider, N., Miller, A. J. & Pierce, D. W. Anatomy of North Pacific decadal variability. *J. Clim.* **15**, 586–605 (2002).
 36. Kwon, Y.-O. & Deser, C. North Pacific decadal variability in the community climate system model version 2. *J. Clim.* **20**, 2416–2433 (2007).
 37. Stuecker, M. F. Revisiting the Pacific meridional mode. *Sci. Rep.* **8**, 3216 (2018).
 38. Kim, H., Kang, S. M., Kay, J. E. & Xie, S.-P. Subtropical clouds key to Southern Ocean teleconnections to the tropical Pacific. *Proc. Natl. Acad. Sci. USA* **119**, e2200514119 (2022).
 39. Wittenberg, A. T., Rosati, A., Delworth, T. L., Vecchi, G. A. & Zeng, F. ENSO modulation: is it decadal predictable? *J. Clim.* **27**, 2667–2681 (2014).
 40. Latif, M. & Barnett, T. P. Causes of decadal climate variability over the North Pacific and North America. *Science* **266**, 634–637 (1994).
 41. Knutson, T. R. & Manabe, S. Time-mean response over the Tropical Pacific to increased CO₂ in a coupled ocean-atmosphere model. *J. Clim.* **8**, 2181–2199 (1995).
 42. Yukimoto, S. et al. ENSO-like interdecadal variability in the Pacific Ocean as simulated in a coupled general circulation model. *J. Geophys. Res.: Oceans* **105**, 13945–13963 (2000).
 43. Jin, F.-F. Low-frequency modes of tropical ocean dynamics*. *J. Clim.* **14**, 3874–3881 (2001).
 44. Meehl, G. A. & Hu, A. Megadroughts in the Indian monsoon region and southwest North America and a mechanism for associated multidecadal Pacific sea surface temperature anomalies. *J. Clim.* **19**, 1605–1623 (2006).
 45. Power, S. & Colman, R. Multi-year predictability in a coupled general circulation model. *Clim. Dyn.* **26**, 247–272 (2006).
 46. Gu, D. & Philander, S. G. H. Interdecadal climate fluctuations that depend on exchanges between the tropics and extratropics. *Science* **275**, 805–807 (1997).
 47. Schneider, N. et al. Pacific thermocline bridge revisited. *Geophys. Res. Lett.* **26**, 1329–1332 (1999).
 48. Munk, W. Internal waves and small-scale processes. *Evolution of Physical Oceanography—Scientific Surveys in Honor of Henry Stommel* 264–291 (MIT Press, 1981).
 49. Schneider, N. A decadal spiciness mode in the tropics. *Geophys. Res. Lett.* **27**, 257–260 (2000).
 50. Yeager, S. G. & Large, W. G. Late-winter generation of spiciness on subducted isopycnals. *J. Phys. Oceanogr.* **34**, 1528–1547 (2004).
 51. Zeller, M., McGregor, S., Sebille, E., van, Capotondi, A. & Spence, P. Subtropical-tropical pathways of spiciness anomalies and their impact on equatorial Pacific temperature. *Clim. Dyn.* **56**, 1131–1144 (2021).
 52. San, S.-C. & Tseng, Y. Aleutian low/PDO forces a decadal subsurface spiciness propagating mode in the North Pacific. *Clim. Dyn.* 1–19. <https://doi.org/10.1007/s00382-023-06938-w> (2023).
 53. McPhaden, M. J. & Zhang, D. Slowdown of the meridional overturning circulation in the upper Pacific Ocean. *Nature* **415**, 603–608 (2002).
 54. McPhaden, M. J. & Zhang, D. Pacific Ocean circulation rebounds. *Geophys. Res. Lett.* **31**, L18301 (2004).
 55. Zhang, D. & McPhaden, M. J. Decadal variability of the shallow Pacific meridional overturning circulation: relation to tropical sea surface temperatures in observations and climate change models. *Ocean Model.* **15**, 250–273 (2006).
 56. Capotondi, A. & Qiu, B. Decadal variability of the Pacific shallow overturning circulation and the role of local wind forcing. *J. Clim.* **36**, 1001–1015 (2023).
 57. Cai, W. et al. Pantropical climate interactions. *Science* **363**, eaav4236 (2019).
 58. Kucharski, F., Kang, I. S., Farneti, R. & Feudale, L. Tropical Pacific response to 20th century Atlantic warming. *Geophys. Res. Lett.* **38**, L03702 (2011).

59. Kucharski, F. et al. Atlantic forcing of Pacific decadal variability. *Clim. Dyn.* **46**, 2337–2351 (2015).
60. Li, X., Xie, S.-P., Gille, S. T. & Yoo, C. Atlantic-induced pan-tropical climate change over the past three decades. *Nat. Clim. Chang.* **6**, 275–279 (2015).
61. Meehl, G. A. et al. Atlantic and Pacific tropics connected by mutually interactive decadal-timescale processes. *Nat. Geosci.* 1–7 <https://doi.org/10.1038/s41561-020-00669-x> (2020).
62. Ruprich-Robert, Y. et al. Impacts of Atlantic multidecadal variability on the tropical Pacific: a multi-model study. *Npj Clim. Atmos. Sci.* **4**, 33 (2021).
63. Kim, W. M., Yeager, S. & Danabasoglu, G. Atlantic multidecadal variability and associated climate impacts initiated by ocean thermohaline dynamics. *J. Clim.* **33**, 1317–1334 (2019).
64. O'Reilly, C. H. et al. Challenges with interpreting the impact of Atlantic multidecadal variability using SST-restoring experiments. *npj Clim. Atmos. Sci.* **6**, 14 (2023).
65. Deser, C. & Phillips, A. S. Spurious Indo-Pacific connections to internal Atlantic multidecadal variability introduced by the global temperature residual method. *Geophys. Res. Lett.* **50**, e2022GL100574 (2023).
66. Zhao, Y. & Capotondi, A. The role of the tropical Atlantic in tropical Pacific climate variability. *npj Clim. Atmos. Sci.* **7**, 140 (2024).
67. Luo, J.-J., Sasaki, W. & Masumoto, Y. Indian Ocean warming modulates Pacific climate change. *Proc. Natl Acad. Sci. USA* **109**, 18701–18706 (2012).
68. Dong, L. & McPhaden, M. J. Why has the relationship between Indian and Pacific Ocean decadal variability changed in recent decades? *J. Clim.* **30**, 1971–1983 (2017).
69. Gao, X. et al. Origins of multidecadal SST variations in the southern Atlantic and Indian Oceans since the 1960s. *Geophys. Res. Lett.* **50**, e2022GL101735 (2023).
70. Ding, Y. et al. Emergence of decadal linkage between Western Australian coast and Western-central tropical Pacific. *Nat. Commun.* **15**, 4458 (2024).
71. Meehl, G. A., Hu, A. & Tebaldi, C. Decadal prediction in the Pacific region. *J. Clim.* **23**, 2959–2973 (2010).
72. Timmreck, C., Pohlmann, H., Illing, S. & Kadow, C. The impact of stratospheric volcanic aerosol on decadal-scale climate predictions. *Geophys. Res. Lett.* **43**, 834–842 (2016).
73. Ménégoz, M., Bilbao, R., Bellprat, O., Guemas, V. & Doblas-Reyes, F. J. Forecasting the climate response to volcanic eruptions: prediction skill related to stratospheric aerosol forcing. *Environ. Res. Lett.* **13**, 064022 (2018).
74. Wu, X., Yeager, S. G., Deser, C., Rosenbloom, N. & Meehl, G. A. Volcanic forcing degrades multiyear-to-decadal prediction skill in the tropical Pacific. *Sci. Adv.* **9**, eadd9364 (2023).
75. Bilbao, R. et al. Impact of volcanic eruptions on CMIP6 decadal predictions: a multi-model analysis. *Earth Syst. Dyn. Discuss.* **2023**, 1–34 (2023).
76. Meehl, G. A. & Teng, H. Case studies for initialized decadal hindcasts and predictions for the Pacific region. *Geophys Res Lett.* **39**, n/a–n/a (2012).
77. Meehl, G. A., Hu, A. & Teng, H. Initialized decadal prediction for transition to positive phase of the Interdecadal Pacific Oscillation. *Nat. Commun.* **7**, 11718 (2016).
78. Pohlmann, H., Kröger, J., Greatbatch, R. J. & Müller, W. A. Initialization shock in decadal hindcasts due to errors in wind stress over the tropical Pacific. *Clim. Dyn.* **49**, 2685–2693 (2017).
79. Teng, H., Meehl, G. A., Branstator, G., Yeager, S. & Karspeck, A. Initialization shock in CCSM4 decadal prediction experiments. *Glob. Chang. Mag.* **25**, 41–46 (2017).
80. Yeager, S. G. et al. Reduced Southern Ocean warming enhances global skill and signal-to-noise in an eddy-resolving decadal prediction system. *npj Clim. Atmos. Sci.* **6**, 107 (2023).
81. Boer, G. J., Khari, V. V. & Merryfield, W. J. Decadal predictability and forecast skill. *Clim. Dyn.* **41**, 1817–1833 (2013).
82. Wu, X., Okumura, Y. M., DiNezio, P. N., Yeager, S. G. & Deser, C. The equatorial Pacific cold tongue bias in CESM1 and its influence on ENSO forecasts. *J. Clim.* **35**, 3261–3277 (2022).
83. Sun, Z. et al. The impact of wind corrections and ocean-current influence on wind stress forcing on the modeling of Pacific North Equatorial Countercurrent. *Ocean Model.* **166**, 101876 (2021).
84. Bretherton, C. S., Smith, C. & Wallace, J. M. An intercomparison of methods for finding coupled patterns in climate data. *J. Clim.* **5**, 541–560 (1992).
85. Zhao, Y., Di Lorenzo, E., Newman, M., Capotondi, A. & Stevenson, S. A Pacific tropical decadal variability challenge for climate models. *Geophys. Res. Lett.* **50**, e2023GL104037 (2023).
86. McGregor, S., Stuecker, M. F., Kajtar, J. B., England, M. H. & Collins, M. Model tropical Atlantic biases underpin diminished Pacific decadal variability. *Nat. Clim. Chang.* **8**, 493–498 (2018).
87. Kim, W. M., Yeager, S. G., Danabasoglu, G. & Chang, P. Exceptional multi-year prediction skill of the Kuroshio Extension in the CESM high-resolution decadal prediction system. *npj Clim. Atmos. Sci.* **6**, 118 (2023).
88. Zhang, Q. et al. Enhanced Atlantic meridional mode predictability in a high-resolution prediction system. *Sci. Adv.* **10**, eado6298 (2024).
89. Boer, G. J. et al. The decadal climate prediction project (DCPP) contribution to CMIP6. *Geosci. Model Dev.* **9**, 3751–3777 (2016).
90. Griffies, S. M. et al. OMIP contribution to CMIP6: experimental and diagnostic protocol for the physical component of the Ocean Model Intercomparison Project. *Geosci. Model Dev.* **9**, 3231–3296 (2016).
91. Hurrell, J. W. et al. The community earth system model: a framework for collaborative research. *Bull. Am. Meteorol. Soc.* **94**, 1339–1360 (2013).
92. Kay, J. et al. The Community Earth System Model (CESM) large ensemble project: a community resource for studying climate change in the presence of internal climate variability. *Bull. Am. Meteorol. Soc.* **96**, 1333–1349 (2015).
93. Neale, R., Chen, C. & Note, G. A. Description of the NCAR community atmosphere model (CAM 5.0). (2010).
94. Smith, R. et al. The parallel ocean program (POP) reference manual ocean component of the community climate system model (CCSM) and community earth system model (CESM). *LAUR-01853*, **141**, 1–140 (UCAR, 2010).
95. Lawrence, D. M. et al. Parameterization improvements and functional and structural advances in version 4 of the Community Land Model. *J. Adv. Model. Earth Syst.* **3**, M03001 (2011).
96. Hunke, E. C. & Lipscomb, W. H. CICE: The Los Alamos sea ice model, documentation and software, version 4.0. *Los Alamos National Laboratory Technical Report LA-CC-06-012*. 76 pp. (2008).
97. Capotondi, A., Deser, C., Phillips, A., Okumura, Y. & Larson, S. ENSO and Pacific decadal variability in the Community Earth System Model version 2. *J. Adv. Model. Earth Syst.* <https://doi.org/10.1029/2019ms002022> (2020).
98. Yeager, S. G., Karspeck, A. R. & Danabasoglu, G. Predicted slowdown in the rate of Atlantic sea ice loss: Predicted rate of sea ice loss. *Geophys. Res. Lett.* **42**, 10,704–10,713 (2015).
99. Meehl, G. A. et al. The effects of bias, drift, and trends in calculating anomalies for evaluating skill of seasonal-to-decadal initialized climate predictions. *Clim. Dyn.* **59**, 3373–3389 (2022).
100. Huang, B. et al. Extended reconstructed sea surface temperature, version 5 (ERSSTv5): upgrades, validations, and intercomparisons. *J. Clim.* **30**, 8179–8205 (2017).
101. Rayner, N. A. et al. Global analyses of sea surface temperature, sea ice, and night marine air temperature since the late nineteenth century. *J. Geophys. Res. Atmos.* **108**, 4407 (2003).
102. Good, S. A., Martin, M. J. & Rayner, N. A. EN4: Quality controlled ocean temperature and salinity profiles and monthly objective

- analyses with uncertainty estimates. *J. Geophys. Res. Oceans* **118**, 6704–6716 (2013).
103. Gouretski, V. & Reseghetti, F. On depth and temperature biases in bathythermograph data: development of a new correction scheme based on analysis of a global ocean database. *Deep Sea Res. Part Oceanogr. Res. Pap.* **57**, 812–833 (2010).
 104. Balmaseda, M. A., Mogensen, K. & Weaver, A. T. Evaluation of the ECMWF ocean reanalysis system ORAS4. *Q. J. R. Meteorol. Soc.* **139**, 1132–1161 (2013).
 105. McDougall, T. J., Jackett, D. R., Wright, D. G. & Feistel, R. Accurate and computationally efficient algorithms for potential temperature and density of seawater. *J. Atmos. Ocean. Technol.* **20**, 730–741 (2003).
 106. Hersbach, H. et al. The ERA5 global reanalysis. *Q. J. R. Meteorol. Soc.* **146**, 1999–2049 (2020).
 107. Slivinski, L. C. et al. Towards a more reliable historical reanalysis: improvements for version 3 of the Twentieth Century Reanalysis system. *Q. J. R. Meteorol. Soc.* **145**, 2876–2908 (2019).
 108. Goddard, L. et al. A verification framework for interannual-to-decadal predictions experiments. *Clim. Dyn.* **40**, 245–272 (2013).
 109. Large, W. G., Danabasoglu, G., Doney, S. C. & McWilliams, J. C. Sensitivity to surface forcing and boundary layer mixing in a global ocean model: annual-mean climatology. *J. Phys. Oceanogr.* **27**, 2418–2447 (1997).
 110. Capotondi, A. & Alexander, M. A. Rossby waves in the tropical North Pacific and their role in decadal thermocline variability. *J. Phys. Oceanogr.* **31**, 3496–3515 (2001).
 111. Capotondi, A., Alexander, M. A. & Deser, C. Why are there Rossby wave maxima in the Pacific at 10°S and 13°N? *J. Phys. Oceanogr.* **33**, 1549–1563 (2003).
- statements, findings, conclusions, and recommendations are those of the author(s) and do not necessarily reflect the views of the National Oceanic and Atmospheric Administration, or the U.S. Department of Commerce. S.G.Y. acknowledges support from award NA20OAR4310408 of the Climate Variability and Predictability program of NOAA's Climate Program Office. A.C. was supported by the NOAA Climate Program Office Climate Variability and Predictability Program and by DOE Award # DE-SC0023228. PMEL contribution no. 5636.

Author contributions

X.W. conceptualized the study, conducted the analysis with detailed discussions with S.G.Y. and C.D., and wrote the initial draft. All authors contributed to interpreting the results and editing the manuscript.

Competing interests

The authors declare no competing interests.

Additional information

Supplementary information The online version contains supplementary material available at <https://doi.org/10.1038/s41612-024-00851-7>.

Correspondence and requests for materials should be addressed to Xian Wu.

Reprints and permissions information is available at <http://www.nature.com/reprints>

Publisher's note Springer Nature remains neutral with regard to jurisdictional claims in published maps and institutional affiliations.

Open Access This article is licensed under a Creative Commons Attribution 4.0 International License, which permits use, sharing, adaptation, distribution and reproduction in any medium or format, as long as you give appropriate credit to the original author(s) and the source, provide a link to the Creative Commons licence, and indicate if changes were made. The images or other third party material in this article are included in the article's Creative Commons licence, unless indicated otherwise in a credit line to the material. If material is not included in the article's Creative Commons licence and your intended use is not permitted by statutory regulation or exceeds the permitted use, you will need to obtain permission directly from the copyright holder. To view a copy of this licence, visit <http://creativecommons.org/licenses/by/4.0/>.

© The Author(s) 2024

Acknowledgements

We would like to thank the three anonymous reviewers for their constructive comments and suggestions. We thank Elizabeth Maroon for helpful discussion on the design of the regional initialization experiments, and Nan Rosenbloom for providing the example scripts to run the CESM1 decadal forecasts. We thank Ping Chang and Who Kim for their insightful comments and suggestions on our analysis. We also thank Liping Zhang for her helpful comments on the manuscript. The CESM project is supported primarily by the National Science Foundation (NSF). The National Center for Atmospheric Research (NCAR) is a major facility sponsored by the NSF under Cooperative Agreement 1852977. X.W. was supported by an Advanced Study Program postdoctoral fellowship from NCAR and was supported by the Cooperative Institute for Modeling the Earth System (CIMES) award NA23OAR4320198 from the National Oceanic and Atmospheric Administration, U.S. Department of Commerce. The